Asian Journal of Chemistry; Vol. 37, No. 10 (2025), 2406-2414
ASIAN JOURNAL OF CHEMISTRY
https://doi.org/10.14233/ajchem.2025.34280

Structural, Supramolecular, Crystal Engineering Insight of (4-Ethyl-9-(phenylsulfonyl)-9*H*-carbazole-2,3-diyl)*bis*(phenylmethanone) Derivative

M.V. MUPPULI[1], K. RAJESH[1,2,*], P. KURINJINATHAN[3], V. MOHAN KUMAR[3], K. GAYATHRI[1] and V. THAYANITHI[4]

[1]Department of Physics, Centre for Hydrogen Energy Research (HER), Academy of Maritime Education and Training, Kanathur-603112, India
[2]Department of Physics, Dayananda Sagar College of Engineering, Bengaluru-560111, India
[3]Department of Physics, PSG college of Arts and Science, Coimbatore-641014, India
[4]Department of Physics, Nandha Engineering College, Erode-638052, India

*Corresponding author: E-mail: krishjayarajesh@gmail.com

Received: 17 June 2025 *Accepted*: 1 September 2025 *Published online*: 30 September 2025 AJC-22124

Structural, intermolecular interaction and electronic effects of a novel (4-ethyl-9-(phenylsulfonyl)-9*H*-carbazole-2,3-diyl)*bis*(phenylmethanone) derivatives were systematically investigated through single crystal X-ray diffraction studies, density functional theory (DFT) calculations and the Hirshfeld surface analysis techniques. The compound crystallized with the space group of $P2_1/n$ in the monoclinic crystal structure. The compound crystallizes in a planar conformation, stabilized by non-covalent interactions like van der Waals forces and C–H···O hydrogen bonds. Hirshfeld surface analysis quantitatively revealed the nature and extent of these supramolecular interactions, providing insight into the crystal packing behaviour. DFT studies were employed to evaluate the molecular orbitals arrangements, energy gap and electrostatic potential of molecules, offering an understanding of the electronic structure and potential reactivity of the titled compound. The experimental and theoretical values were in good agreement, confirming the stability and planarity of the molecule. In addition, the molecular docking studies demonstrated significant binding affinity of the compound towards target proteins of *Escherichia coli* ThDP–dependent enzyme, indicating promising pharmacological potential. These findings contribute to the growing interest in carbazole-based compounds as multifunctional materials in both medicinal and material chemistry.

Keywords: Carbazole, Hirshfeld surface analysis, Molecular electrostatic potential, Density functional theory, Binding affinity.

INTRODUCTION

Recent developments in non-linear optical (NLO) materials have attracted significant attention from both theoretical and experimental researchers worldwide, owing to their vast potential applications [1,2]. Numerous technological advancements have been driven by NLO materials. The pursuit of high performance NLO devices has, in turn, fueled the development of novel molecules with enhanced data transfer capabilities [3]. Optoelectronic devices such as organic light-emitting diodes (OLEDs), organic photovoltaics (OPVs), dye-sensitized solar cells (DSSCs), sensors and photodetectors leverage NLO properties to perform a diverse range of functions [4]. Organic molecules, in particular, exhibit a high nonlinear optical (NLO) response, making them highly suitable for efficient electro-optic modulation. Hence, the development of a new molecule containing NLO responses is essential for the exigency of society [5].

Carbazoles are important aromatic tricyclic compounds with conjugated π-electron systems. Due to the π-conjugation carbazole based compounds exhibits high polarizability and significant non-linear absorption in the visible and infrared spectra [6,7]. It shows good photophysical properties and easy functionalization of the carbazole core at 3-, 6- and 9-positions by covalently linking to other molecules make them applicable in various potential applications [8]. Thus, the push-pull chromophores could be tailor-made for better NLO properties by modulating the D-π-A system thereby perturbing the π-electron delocalization of the local excited state attained by absorption of photons leading to intramolecular charge transfer (ICT) [9,10]. Creating an effective synthesis of the substantial work on carbazole derivatives has been a major focus of our laboratory efforts.

The entire potential of these materials in the sector is being actively investigated *via* ongoing research, which includes the development of new derivatives and the improvement of

device topologies. In this regard, our team make efforts to develop a plan for the effective synthesis of (4-ethyl-9- (phenylsulfonyl)-9*H*-carbazole-2,3-diyl)*bis*(phenylmethanone) by a new synthesis method. Geometrical structure density functional theory (DFT) was utilized to augment the evaluation of their physical attributes by determining their crystal structure using single crystal XRD and their suitability for possible optoelectronic applications. The investigations on the HOMO-LUMO gap, molecular docking, polarizability and physicochemical were also carried out.

EXPERIMENTAL

Synthesis of (4-ethyl-9-(phenylsulfonyl)-9*H*-carbazole -2,3-diyl)*bis*(phenylmethanone): A mixture of 2-bromomethylindole (0.30 g in 0.74 mmol) and triphenylphospine (0.21 g in 0.81 mmol) was stirred in 15 mL of dehydrated DMF at room temperature for continuously 4 h under a nitrogen gas atmosphere to attained the corresponding phosphonium salt. Followed by the crude phosphonium salt was subjected to annulation with dibenzoylacetylene (0.21 g, 0.89 mmol) with potassium carbonate (0.20 g, 1.48 mmol) as a base at normal room temperature for 6 h (**Scheme-I**). Subsequently, at the end of reaction, standard aqueous workup followed by crystallization from 10 mL of methanol provided the required carbazole derivative as a colourless solid material of 0.35 g with 88% purity with the melting point 208 to 210 ºC.

X-ray crystallography

Data collection and reduction: X-ray diffraction data for the title compound were collected using a Bruker SMART APEXII CCD diffractometer [11] at the in-house GNR X-ray Facility Center. The instrument employed graphite monochromated Mo*K*α radiation (λ = 0.7107 Å) and a CCD detector for data acquisition. Sums of 11,024 reflections were recorded, from which 2,935 unique reflections were identified and used for the structural solution. Data integration, intensity extraction and frame processing were performed using the SAINT software package [12], which also applied Lorentz and polarization (Lp) corrections, as well as decay correction. An empirical absorption correction was applied using the SADABS program *via* a multi-scan method, ensuring improved data quality and reliability [13,14].

Computational analysis: The Gaussian 09, Revision D.01 software program was used for all quantum chemistry computations. The ground-state geometry of the title compound was optimized using the B3LYP functional in conjunction with the 6-311++G(d,p) basis set, in absence of imposing any symmetry constraints. To evaluate the non-linear optical (NLO) properties, including first-order hyperpolarizability, further calculations were performed using multiple exchange-correlation functionals: B3LYP, BH&HLYP and the range-separated CAM-B3LYP functional [15]. These were combined with a triple-basis set, 6-311++G(d,p), to ensure better accuracy in describing the electronic distribution. Solvent effects on the electronic properties and stability of the molecule were analyzed using the self-consistent reaction field (SCRF) method within the polarizable continuum model (PCM) framework [16], as implemented in Gaussian 09. Calculations were performed in different polarity solvents to assess the influence of the dielectric environment on the compound's geometry and optical response.

Structure solution and refinement: The Bruker AXS KAPPA APEX3-CMOS diffractometer was used to gather raw intensity data at the upper limit of θ = 24.998º after single crystals were subjected to diffraction using characteristic X-ray, *K*α of the Mo target of wavelength, 0.71073 Å. Unit cell refinement computations, data reduction and integration were performed using APEX2 and SAINT [11]. In cell parameter measurements, 6798 reflections were useful following the use of Lorentz and polarization adjustments. Single-crystal X-ray diffraction data of FPMPM were used to solve the crystal structure using the direct methods of SHELXS97 [17]. The structural model was refined using 1486 reflections out of the 2071 independent reflections that satisfied $I > 2\sigma(I)$ within the maximum θ value of 24.998º. The data were refined using SHELXL-2014 to minimize the full-matrix least-squares on F^2 [18]. Uiso (H) = 1.5*Ueq (C_{methyl}) or 1.2*Ueq(C) in riding mode were used to refine the geometrically positioned H atoms (C single bond H = 0.93–0.97 Å) and their parameters were limited. Electron densities were used to determine the torsion angles for methyl H. With S = 1.068, the structure model's final refinement produced 147 refined parameters at convergence of R1 to 0.0547 and wR2 to 0.1381. The chemical, ORTEP and packing diagrams were crafted using Platon [19] and ORTEP [20].

NMR analysis: ^{1}H NMR spectral data of the carbazole derivative was observed at 300 MHz in $CDCl_3$ solvent. The spectrum provides the characteristic signals consistent with a

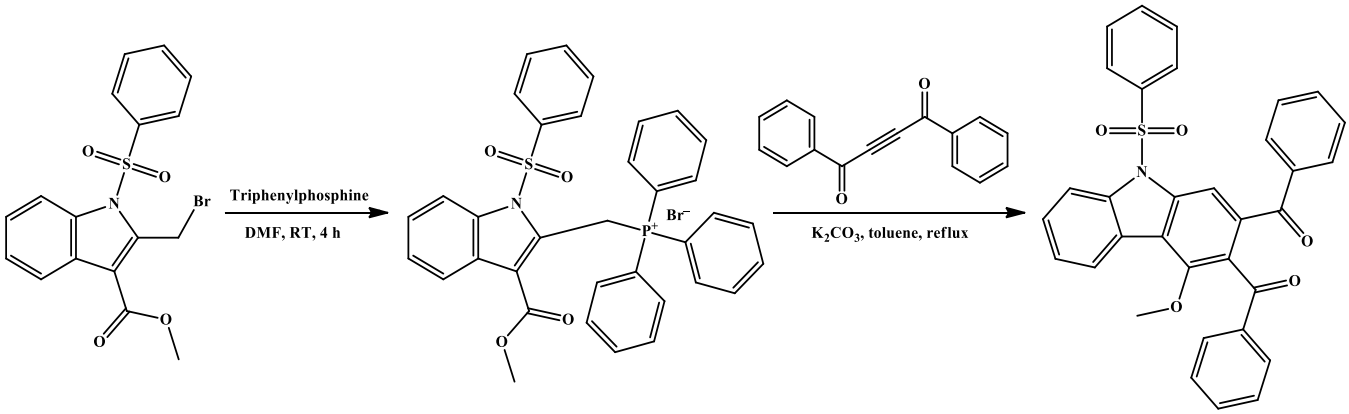

Scheme-I

polycyclic aromatic system holding the phenyl substituents and the ethyl group; it is likely joined to nitrogen or a aromatic ring, as inferred from the chemical shift and coupling patterns. The ^{13}C NMR of the title compound was recorded at 75 MHz range in $CDCl_3$.

Density functional theory (DFT): The 3D structure of titled compound was generated using Gauss View 5 [21]. The conformational analyses were performed to identify the stable geometry of the structure. Geometry optimization was done using the B3LYP functional in conjugation with the proper basis sets. The B3LYP functional, which incorporates Becke's exchange [22] and Lee-Yang-Parr correlation functions, has proven effective in determine the π-conjugated systems such as carbazole scaffolds. The performance of functional groups is assessed and recent advancements in the exchange correlation functional are reported.

Hirshfeld surface and fingerprint plot analysis: The crystal explorer application was used to generate Hirshfeld surfaces (HS) and fingerprint plots for the title compounds [23]. In the figures, white indicates lengths close to the van der Waals (vdW) separation, blue indicates longer distances and red indicates distances closer than the sum of the vdW radii. The various types of molecular interactions are mostly depicted in 2D fingerprint plots, which provide the quantitative data on the unique contributions of all interactions in crystal packing. Molecular electrostatic potential (MEP) surfaces mapped into the Hirshfeld surfaces at the HF/3-21G level of theory gives the information into the electrostatic complementarily in the lattice plane.

HOMO–LUMO analysis: HOMO and LUMO are the key quantum chemical characteristics for determining molecular interactions with other species, as well as characterizing the molecule's chemical reactivity, global hardness, softness and kinetic stability [24]. HOMO–LUMO analysis provides the information about the occupied level of molecules and atoms. The lowest unfilled orbital (LUMO), the next empty orbital (LUMO+1) and the highest occupied molecular orbital (HOMO) can be identify using the analysis.

Molecular docking: Molecular computations are used to examine comprehensively the interactions of the ligand with active site residues [25,26]. The standard cutoff estimates for hydrogen bonds are 3 Å (dH-X) and for van der Waals interactions, 6.0 Å was chosen. Each inhibitor has a fixed number of docked postures of 100. If a ligand's top three binding conformations fell within 1.5 Å RMSD, early termination was allowed. Followed by the docking process, the ligand's distinct binding poses were detected and their interactions with the specific protein molecule through hydrogen bonds were measured.

RESULTS AND DISCUSSION

Crystal structure of (4-ethyl-9-(phenylsulfonyl)-9*H*-carbazole-2,3-diyl)*bis*(phenylmethanone): The optimized geometry of the structural model shown in Fig. 1 is illustrated through the molecule's ORTEP diagram, based on crystallographic experimental data. Table-1 provides a summary of the crystal data and structure refinement figure. In the titled compound ($C_{33}H_{23}NO_5S$), the carboxylate ring system (C1–C12/N1) (RMS deviation of 0.038 Å unit) has dihedral angles of 52.80(10)º and 78.71(11)º with the lattice planes of the two phenylmethanone (O3/C26-C32) and (O4/C19-C25), respectively and is inclined to each other at an angle of 56.73(12)º. For comparable, the bond lengths of N1–C6 = 1.4337(5) Å and N1–C = 1.355(14) Å have been reported in Table-2, which is due to the phenylsulfonyl group's electron-drawing nature.

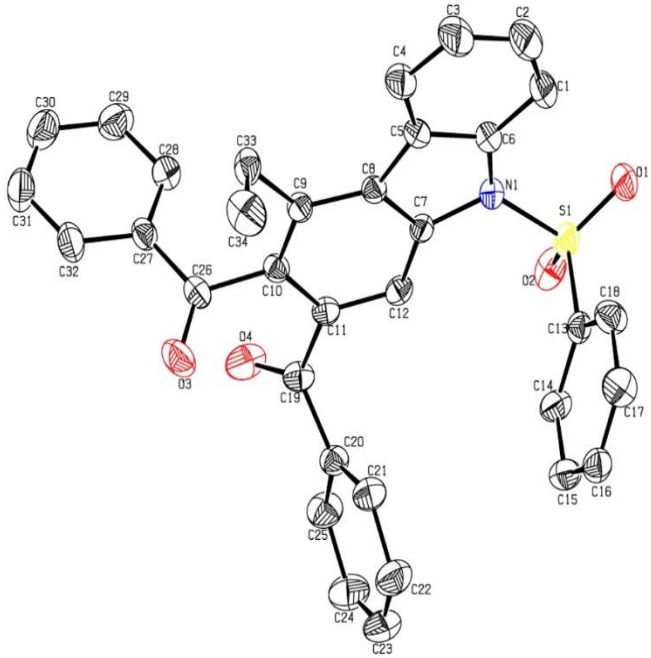

Fig. 1. ORTEP diagram of title compound

TABLE-1
THE EXPERIMENTAL, CRYSTAL DATA AND STRUCTURE REFINEMENT VALUES OF THE DERIVATIVE

Parameters	Values
Empirical formula	$C_{33}H_{23}NO_5S$
Formula weight	545.58
Temperature	296(2) K
Wavelength	0.71073 A
Crystal system, space group	Monoclinic, P $2_1/n$
Unit cell dimensions	a = 11.026(3) Å; α = 90º b = 9.557(3) Å; β= 99.768(9)º c = 26.833(6) Å; γ = 90º
Volume	2786.7(12) A^3
Z, Calculated density	4, 1.300 Mg/m^3
Absorption coefficient	0.159 mm^{-1}
F(000)	1136
Crystal size	0.180 × 0.150 × 0.120 mm
θ range for data collection	2.630º to 33.192º
Limiting indices	-16 <= *h* <= 16, -14 <= *k* <= 14, -41 <= *l* <= 36
Reflections collected/unique	69263/10497 [R(int) = 0.0500]
Completeness to θ = 25.242	99.60%
Refinement method	Full-matrix least-squares on F^2
Data/restraints/parameters	10497/0/362
Goodness-of-fit on F^2	1.136
Final R indices [I>2σ(I)]	R1 = 0.1045, wR2 = 0.2257
R indices (all data)	R1 = 0.1496, wR2 = 0.2687
Extinction coefficient	0.313(15)
Largest diff. peak and hole	1.326 and -1.466 e.A^{-3}

TABLE-2
GEOMETRICAL PARAMETERS OF BOND LENGTH (Å)

Bond length	Values	Bond length	Values
C1-C2	1.381(5)	C17-C18	1.393(3)
C1-C6	1.390(3)	C19-O4	1.217(2)
C2-C3	1.388(5)	C19-C20	1.491(3)
C3-C4	1.379(3)	C20-C21	1.393(3)
C4-C5	1.402(3)	C20-C25	1.401(3)
C5-C6	1.405(3)	C21-C22	1.413(4)
C5-C8	1.457(2)	C22-C23	1.380(5)
C6-N1	1.434(3)	C23-C24	1.372(5)
C7-C12	1.383(3)	C24-C25	1.384(4)
C7-N1	1.418(2)	C26-O3	1.222(2)
C7-C8	1.419(2)	C26-C27	1.491(3)
C8-C9	1.401(2)	C27-C28	1.395(3)
C9-C10	1.404(2)	C27-C32	1.399(3)
C9-C33	1.520(3)	C28-C29	1.378(3)
C10-C11	1.417(2)	C29-C30	1.382(5)
C10-C26	1.508(3)	C30-C31	1.392(5)
C11-C12	1.392(3)	C31-C32	1.371(4)
C11-C19	1.501(2)	C33-C34	1.521(4)
C13-C18	1.382(3)	N1-S1	1.6725(17)
C13-C14	1.387(3)	O1-S1	1.4240(18)
C13-S1	1.7579(19)	O2-S1	1.4331(19)
C14-C15	1.387(3)	C16-C17	1.381(4)
C15-C16	1.368(3)		

The optimized structure of the carboxylate compound obtained through DFT calculations is presented in Fig. 2 at the B3LYP/6-311G(d,p) level. The molecule shows a conjugated π-system with variety of functional groups contributing to electronic delocalization. The crystallographic investigation of puckering [27] and asymmetry parameters [28] demonstrates that the thiophene ring has a planar shape. The crystallographic values and other crystal data are listed in Table-1.

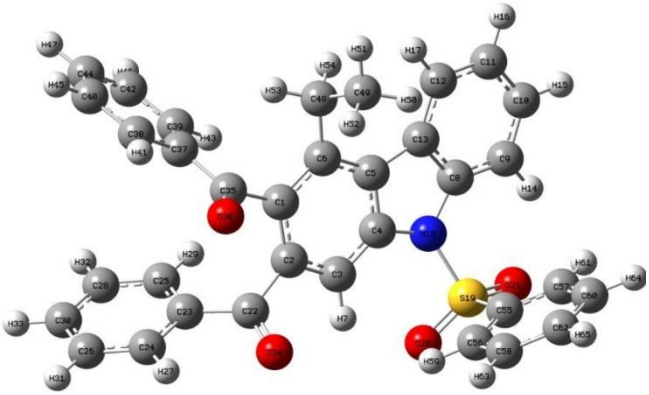

Fig .2. Optimized molecular structure of synthesized molecule using gauss view software

Atom S1 is in a deformed tetrahedral structure as the Thorpe-Ingold effect [29] is responsible for the broadening of angle O1–S1–O2 = 120.30(1) and narrowing of angle N2–S1–C14 = 106.83 (1) from the ideal tetrahedral value (Table-3). The C13-S1 bond length of 1.7579(6) Å in the present structures is comparable to the distances of 1.793 (3) and 1.798 (3) Å in methyl 6-benzoyl-3,5-diphenyl-1,4-thiazine-2-carboxylate-1,1-dioxide [30] and 1.795 (3) and 1.795 (2) Å in thiazine-3-one [31].

TABLE 3
GEOMETRICAL PARAMETERS OF BOND ANGLE (º)

Bond angle	Values	Bond angle	Values
C2-C1-C6	117.8(2)	O4-C19-C20	120.72(18)
C1-C2-C3	121.9(2)	O4-C19-C11	119.40(18)
C4-C3-C2	120.6(3)	C20-C19-C11	119.80(16)
C3-C4-C5	118.8(2)	C21-C20-C25	119.3(2)
C4-C5-C6	119.72(19)	C21-C20-C19	121.69(18)
C4-C5-C8	133.37(19)	C25-C20-C19	118.58(19)
C6-C5-C8	106.91(17)	C20-C21-C22	119.4(2)
C1-C6-C5	121.2(2)	C23-C22-C21	120.0(3)
C1-C6-N1	129.3(2)	C24-C23-C22	120.5(2)
C5-C6-N1	109.49(16)	C23-C24-C25	120.4(3)
C12-C7-N1	128.73(16)	C24-C25-C20	120.3(3)
C12-C7-C8	122.41(16)	O3-C26-C27	122.01(18)
N1-C7-C8	108.85(15)	O3-C26-C10	119.20(19)
C9-C8-C7	120.46(15)	C27-C26-C10	118.78(16)
C9-C8-C5	132.02(16)	C28-C27-C32	119.4(2)
C7-C8-C5	107.50(15)	C28-C27-C26	121.49(17)
C8-C9-C10	117.01(15)	C32-C27-C26	119.1(2)
C8-C9-C33	121.62(16)	C29-C28-C27	120.0(2)
C10-C9-C33	121.26(16)	C28-C29-C30	120.3(3)
C9-C10-C11	121.35(16)	C29-C30-C31	119.9(3)
C9-C10-C26	118.98(16)	C32-C31-C30	120.2(3)
C11-C10-C26	119.52(15)	C31-C32-C27	120.1(3)
C12-C11-C10	121.37(16)	C9-C33-C34	111.5(2)
C12-C11-C19	118.87(16)	C7-N1-C6	107.05(15)
C10-C11-C19	119.65(16)	C7-N1-S1	122.99(13)
C7-C12-C11	117.04(16)	C6-N1-S1	125.54(13)
C18-C13-C14	120.57(19)	O1-S1-O2	120.31(11)
C18-C13-S1	119.58(16)	O1-S1-N1	106.09(10)
C14-C13-S1	119.84(15)	O2-S1-N1	106.82(9)
C13-C14-C15	119.4(2)	O1-S1-C13	109.16(10)
C16-C15-C14	120.5(2)	O2-S1-C13	108.63(10)
C15-C16-C17	120.0(2)	N1-S1-C13	104.71(8)
C16-C17-C18	120.6(2)		
C13-C18-C17	118.9(2)		

Crystal packing information: The crystal structure has two intramolecular C–H···O interactions, with independent molecules connected by C–H···O hydrogen bonding form a C20 chain that runs along the b-axis. In the crystal, molecules are linked *via* C–H···O hydrogen bonds, C–H···π interactions and van der Waals forces, resulting in a three-dimensional network as illustrated in Fig. 3 [32]. The title compound's crystal packing as seen along the *b*-axis. The dashed lines represent the hydrogen bonds C–H···O. For clarity, H atoms that are not a part of these interactions have been left out.

^{1}H NMR (300 MHz, $CDCl_3$): The ^{1}H NMR spectrum is shown in Fig. 4. The spectrum consists with a carbazole derivative with multiple phenyl rings and a strong terminal ethyl group on the nitrogen or carbon adjacent to the nitrogen atom. The complex aromatic framework is identifying with the presence of 20 aromatic protons and the characteristic ethyl patterns [33]. The aromatic protons appearing at δ 8.51–8.49 ppm as a multiplet (2H, ArH) are indicative of protons located adjacent to electron-withdrawing groups, likely within a carbazole or a phenyl-substituted indole moiety. A doublet at δ 8.09 ppm (J = 8.1 Hz, 1H, ArH) suggests ortho coupling, characteristic of a substituted aromatic ring such as a mono-substituted benzene [34]. The multiplet observed in the region

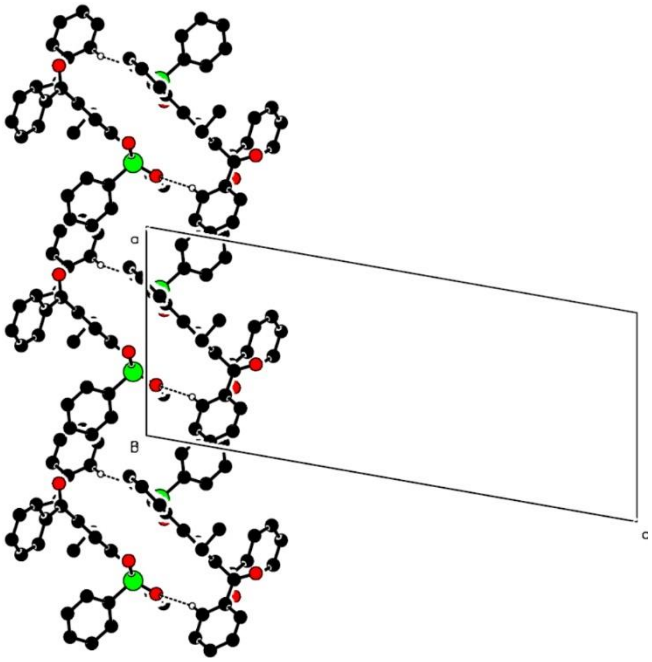

Fig. 3. Packing representation of the crystal

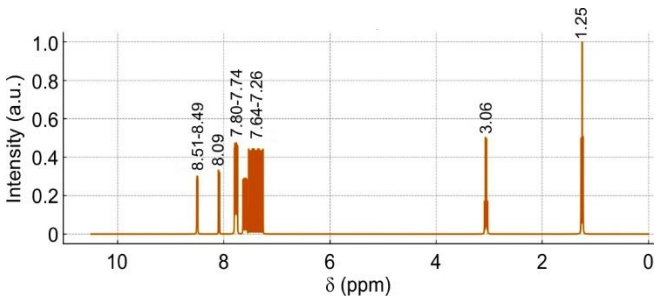

Fig. 4. ^{1}H NMR spectrum of the title compound

δ 7.80–7.74 ppm (6H, ArH) could be attributed to aromatic protons from a triphenylphosphine unit or similar aromatic systems present in the molecule. Another set of aromatic signals appears at δ 7.64–7.56 ppm (3H, ArH), likely arising from aromatic rings contributing to a congested aromatic environment. The broad multiplet in the range δ 7.53–7.26 ppm (8H, ArH) suggests the presence of two or more phenyl rings, or a polyaromatic core structure. In the aliphatic region, a quartet at δ 3.06 ppm (J = 7.5 Hz, 2H, CH_2) corresponds to a methylene group adjacent to a methyl group, while the triplet at δ 1.25 ppm (J = 7.5 Hz, 3H, CH_3) is consistent with a terminal methyl group coupling with the neighbouring methylene group. All the chemical shifts, integration values and multiplicities are well match with the expected structure.

^{13}C NMR ($CDCl_3$, 75 MHz): The ^{13}C NMR spectrum is presented in Fig. 5 and it exhibits 27 distinct carbon signals. It bearing a required number of highly substituted aromatic system consistent of carbonyl functionalities, alkyl side chain and aromatic rings. The 27 carbon signals *viz*. δ 198.0, 195.8, 140.0, 138.7, 138.2, 138.0, 137.7, 137.4, 136.9, 136.1, 134.2, 133.1, 132.9, 130.3, 129.3, 128.4, 128.3, 128.28, 126.9, 126.6, 125.2, 124.6, 123.5, 115.4, 115.2, 24.2, 14.0 ppm. The two distinct downfield peaks at δ 198.0, 195.8 ppm are ketonic carbonyl carbons. The highly dense cluster of peaks observed

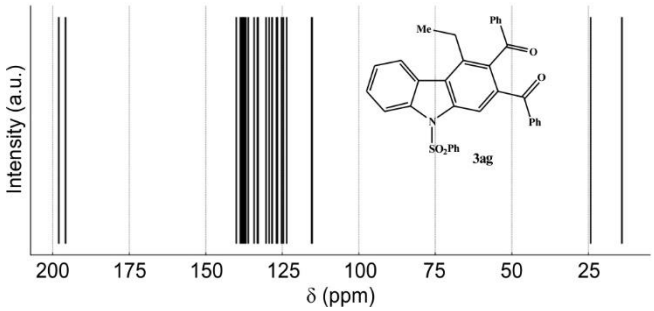

Fig. 5. ^{13}C NMR of the title compound recorded at 75 MHz in $CDCl_3$

between δ 115–140 ppm corresponds to various aromatic and heteroaromatic carbon atoms [35], confirming the presence of a conjugated π-system and phenyl substituents. In addition, the signals at δ 24.2 and δ 14.0 ppm are characteristic of the methylene and methyl carbons of an ethyl group, respectively.

Computational studies

HOMO-LUMO studies: The frontier molecular orbitals (FMOs) of the title carbazole derivative were investigated using density functional theory (DFT) calculations at the B3LYP/6-31G(d) level to gain insights into its electronic structure and potential reactivity. The representations of the HOMO, LUMO and LUMO+1 orbitals are illustrated in Fig. 6. As shown in Fig. 6a, the HOMO is primarily localized over the carbazole moiety and the adjacent conjugated π-system. The distribution of electron density in this region reveals significant π-character, suggesting its potential role as an electron-donating site in intramolecular or intermolecular charge transfer processes. In contrast, Fig. 6b depicts the LUMO, where the electron density is predominantly distributed over the electron-withdrawing substituent and portions of the molecular core. This pattern indicates that the LUMO acts as an electron-accepting region. The spatial separation between the HOMO and LUMO orbitals supports the possibility of an intramolecular charge transfer (ICT) mechanism, a key feature relevant to the compound's performance in optoelectronic applications [36]. Fig. 6c presents the LUMO+1 orbital, which continues to exhibit delocalization over the extended π-conjugated framework and the substituent group. This further confirms the conjugated nature of the molecule and its potential for efficient charge transport. The electronic configuration of the compound reveals that the calculated energy levels of the HOMO and LUMO are –5.445 eV and –3.146 eV, respectively, resulting in an energy gap (ΔE) of 2.299 eV. This relatively small HOMO–LUMO gap plays a crucial role in determining the photophysical and electrochemical behaviour of the molecule [37]. In general, such a narrow band gap is associated with enhanced chemical reactivity and indicates that the compound holds promise for use in organic electronics and the development of nonlinear optical (NLO) devices [38,39].

Electrostatic potential map (ESP): The ESP map (Fig. 7) presents a colour-coded molecular surface indicating regions of varying electrostatic potential. Red areas, particularly on the lower right side, signify high electron density and negative potential, likely due to electronegative atoms such as oxygen, making them favorable sites for electrophilic attack [40]. Blue

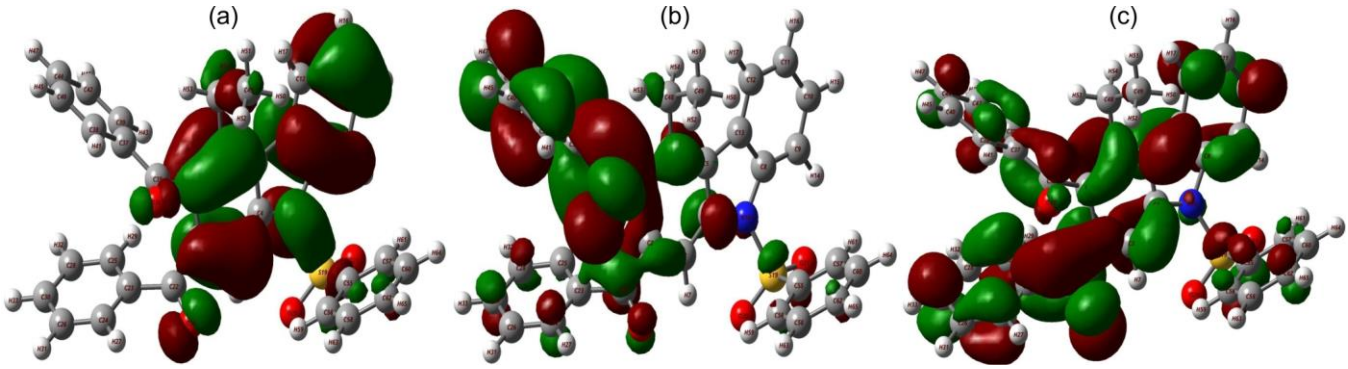

Fig. 6. (a) HOMO orbital, (b) LUMO and (c) LUMO+1 of the synthesized compound

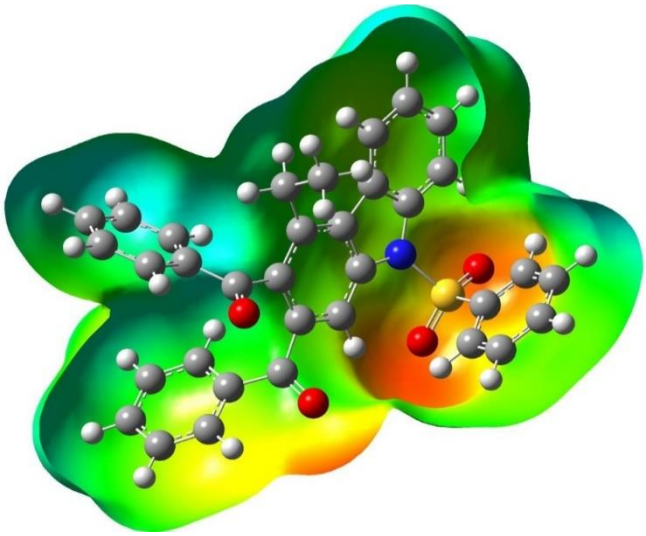

Fig. 7. The MEP surface for (4-ethyl-9-(phenylsulfonyl)-9*H*-carbazole-2,3-diyl)*bis*(phenylmethanone) derivative obtained by B3LYP/6-311G(d,p)

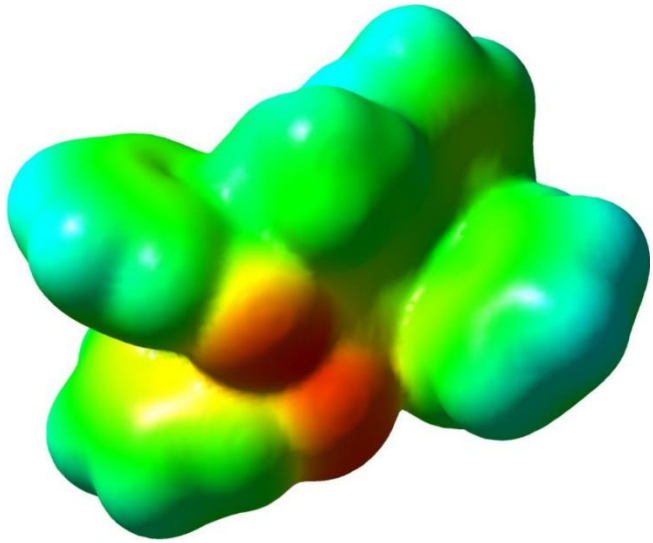

Fig. 8. Mapped surface of the title compound

regions indicate electron-deficient zones, typically near hydrogen atoms, and are susceptible to nucleophilic attack, while green regions represent neutral or low-reactivity zones.

Fig. 8 further highlights strong negative potential around carbonyl and sulfone groups, confirming their potential for electrophilic interactions [41]. In contrast, the carbazole and phenyl rings show a more uniform green-to-light-blue distribution, indicating lower reactivity and a hydrophobic nature.

Overall, the ESP analysis identifies key reactive sites, assisting in understanding the molecule's behaviour in supramolecular interactions, hydrogen bonding and potential biological binding. A summary of its physico-chemical properties is provided in Table-4 [42].

TABLE 4
THE PHYSICO-CHEMICAL PROPERTIES OF THE TITLE COMPOUND

Parameters	Values
HOMO	-5.445 eV
LUMO	-3.146 eV
Energy gap	2.299 eV
HOMO-1	-6.187 eV
LUMO+1	-1.814 eV
(H-1 to L+) Energy gap	4.373 eV
Ionization potential (IP)	5.445 eV
Electron affinity (EA)	3.146 eV
Electrophilicity Index (ω)	4.011
Chemical Potential (μ)	4.295
Electro negativity (χ)	-4.295
Softness (η)	-2.299

Hirshfeld surface analysis: A Hirshfeld surface analysis [43] of the carboxylate complex was conducted to identify the atomic positions capable of forming hydrogen bonds and to quantify the relative contributions of various intermolecular interactions. The calculated values from the analysis include a surface volume of 687.65 Å^3, surface area of 532.31 Å^2, globularity of 0.708 and asphericity of 0.086. Fig. 9 presents the 2D fingerprint plots of the carbazole derivative, mapped over a d_{norm} range from –0.1894 to 1.4759 Å. The normalized contact distance (d_{norm}) was calculated based on both internal (d_i) and external (d_e) distances. Negative d_{norm} values, represented in red, correspond to intermolecular contacts shorter than the sum of van der Waals (vdW) radii, while positive values, shown in blue, indicate contacts longer than the vdW radii. White regions represent contacts at exact vdW distances (d_{norm} = 0), and the grey background depicts the overall molecular surface.

The analysis reveals that the most significant contribution arises from H···H interactions, accounting for 47.6% of the total contacts. This indicates that van der Waals interactions

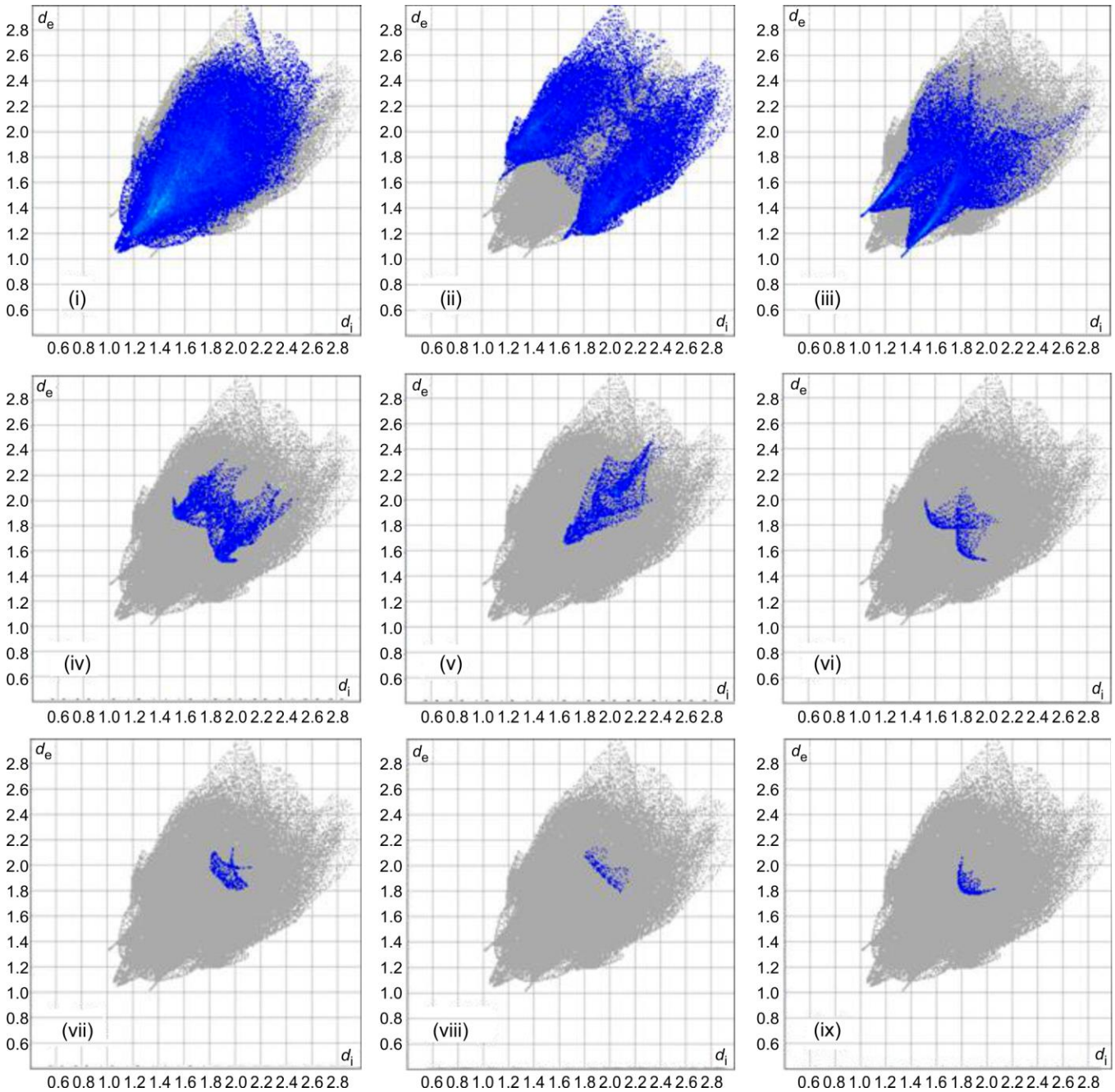

Fig. 9. Two-dimensional fingerprint plots of the carbazole, showing (i) H-H = 47.6%, (ii) C-H = 27.7%, (iii) H-O = 17.8%, (iv) C-O = 3.4%, (v) C-C = 2.2%, (vi) N-O = 0.5%, (vii) C-N = 0.3%, (viii) N-H = 0.2% and (ix) N-N = 0.2% interactions

between hydrogen atoms dominate the packing structure. The C···H interactions contribute 27.7%, suggesting the presence of hydrogen bonding or C–H···π interactions. Furthermore, H···O interactions contribute 17.8%, indicating the potential for conventional hydrogen bonding involving oxygen atoms [44].

Molecular docking studies: Figs. 10 and 11 present the molecular docking report of the titled compound with the active site of the target protein from *E. coli* bacteria. Fig. 10 provides the binding interactions inside the proteins cavity. From this non-covalent bonding such as π-π stacking, hydrogen bonding and hydrophobic connections are evident. This suggests the strong connection between the ligands and active site residues. The titled compound has effective accommodation within the binding pocket; align with the functional groups toward catalytically important amino acids. Fig. 11 represents the docked pose of compound within the three-dimensional active site of *E. coli* protein. This confirms the snug fit and complementarity between the ligands and protein surface [45]. This makes the interactions more stable and improve the inhibit enzymes biological activities like antibacterial, anticancer and antioxidant agents [46].

Table-5 presents the various molecular docking parameters obtained for the interaction between the carbazole derivative and the target protein. The negative docking score and binding affinity values suggest a strong and stable interaction,

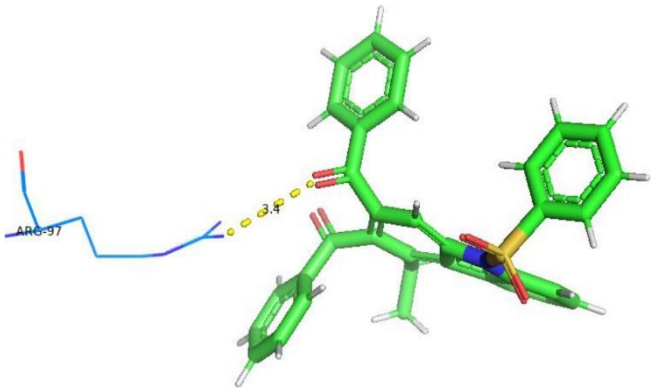

Fig. 10. Molecular docking connections for the carbazole derivative within the binding pocket of *Escherichia coli*

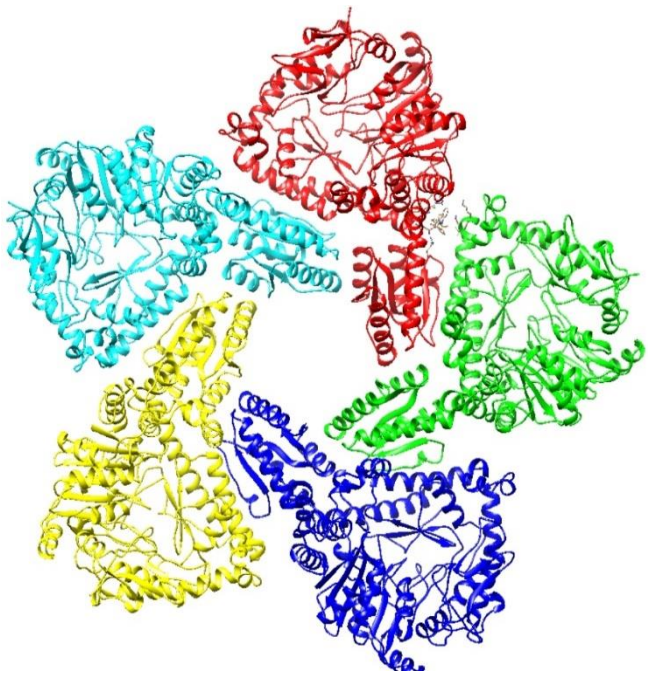

Fig. 11. The docked molecule in the active site pocket of the targeted *Escherichia coli* protein

TABLE-5
MOLECULAR DOCKING INTERACTION SUMMARY OF THE CARBAZOLE DERIVATIVE WITH THE *Escherichia coli* PROTEIN

Docking parameter	Result
Ligands	(4-Ethyl-9-(phenylsulfonyl)-9*H*-carbazole-2,3-diyl)*bis*(phenyl-methanone)derivative
Interaction	ARG97(C-H...O)
Type of interaction	Weak hydrogen bond
Bond distance	3.41 (Å)
Docking score	-7.7263 kcal/mol
Binding affinity	-8.3 Kcal/mol
Estimated inhibition constant (Ki)	0.83 µm
Target protein	*E. coli*
Distance to catalytic site	1.9 (Å)
Docked conformation RMSD	1.2 (Å)
Significance of interaction	Stabilization through weak hydrogen bond in active site pocket

indicating favorable binding of the compound to the active site of the protein. Moreover, the low inhibition constant (K_i) value reflects the titled compound's promising inhibitory potential. Furthermore, the root-mean-square deviation (RMSD) value, which is below 2 Å, confirms the reliability of the predicted docking pose, supporting the validity of the binding conformation.

Polarizability and hyperpolarizability: The first order hyperpolarizability (β) and polarizability (α) of the carbazole derivative were calculated to find out its non-linear optical (NLO) nature. The mean polarizability was calculated to be approximately 255 a.u. This mean polarizability implies a good delocalized π-electron system across the carbazole core. This result suggests that the carbazole derivative has the ability to respond effectively to external electric fields. First order hyperpolarizability (β) was estimated abot 640 a.u. This reflects the accuracy of intramolecular charge transfer in the molecule. The titled molecule in non-centrosymmetric in nature which combined with extended conjugation, helping to its enhancement in NLO response [47].

Conclusion

A novel carboxylate based carbazole derivative ((4-ethyl-9-(phenylsulfonyl)-9*H*-carbazole-2,3-diyl)*bis*(phenylmethanone) derivative was synthesized successfully. The structure of the molecule was computed and explored for its electronic and biological properties. Carboxylate molecule crystallize in the monoclinic space group $P2_1/n$. To solve the molecular structures, a direct methods strategy is employed and the model is refined using full-matrix least-squares processes. The final refining yielded an R-value is 0.10 for the molecule. The stability of the molecule was attributed to the intermolecular C–H···O hydrogen bond. This is further confirmed by Hirshfeld surface analysis in particularly H···H interaction with 47.6%, C···H (27.7%) and H···O (17.8%). The HOMO-LUMO energy gap was calculated to be 2.299 eV, which suggest the better stability with moderate electronic transition capabilities. The molecular docking results show the title compound exhibits a strong binding affinity value of -8.3 Kcal/mol and docking score of -7.73 kcal/mol towards the *E. coli* target protein. This helps the compound for further development as a lead molecule in antibacterial drug design. The value of first order hyperpolarizability (β) and polarizability (α) suggest that the titled compound can be a promising organic nonlinear optical material that can be used in various frequency doubling, optical signal processing units and electro-optic switching applications. Overall, the results strongly suggest that the synthesized molecule exhibits a promising scaffold for various pharmacological exploration and advanced NLO material development.

CONFLICT OF INTEREST

The authors declare that there is no conflict of interests regarding the publication of this article.

REFERENCES

1. H. Wang, M. Mutailipu, Z. Yang, S. Pan and J. Li, *Angew. Chem.*, **137**, e202420526 (2025); https://doi.org/10.1002/ange.202420526

2. M. Khalid, A. Ali, R. Jawaria, M.A. Asghar, S. Asim, M.U. Khan, R. Hussain, M. Fayyaz ur Rehman, C.J. Ennis and M.S. Akram, *RSC Adv.*, **10**, 22273 (2020); https://doi.org/10.1039/D0RA02857F
3. P.K. Samanta, M.M. Alam, R. Misra and S.K. Pati, *Phys. Chem. Chem. Phys.*, **21**, 17343 (2019); https://doi.org/10.1039/C9CP03772A
4. N. Vishwakarma, P.S. Patil and N. Sekar, *ChemistrySelect*, **9**, e202404228 (2024); https://doi.org/10.1002/slct.202404228
5. K.J. Nakum, K.D. Katariya, M. Hagar and R.N. Jadeja, *J. Mol. Struct.*, **1261**, 132891 (2022); https://doi.org/10.1016/j.molstruc.2022.132891
6. A.J. Garza, O.I. Osman, N.A. Wazzan, S.B. Khan, A.M. Asiri and G.E. Scuseria, *Theor. Chem. Acc.*, **133**, 1458 (2014); https://doi.org/10.1007/s00214-014-1458-9
7. H.J. Knölker and K.R. Reddy, *Chem. Rev.*, **102**, 4303 (2002); https://doi.org/10.1021/cr020059j
8. M.V. Muppuli, K. Rajesh, D. Anitha Rexalin, K. Anandan, A. Mani, K. Gayathri, P. Devendran, V. Thayanithi, P. Kurinjinathan and M. Suresh Kumar, *J. Struct. Chem.*, **65**, 987 (2024); https://doi.org/10.1134/S0022476624050123
9. K. Choroba, J. Palion-Gazda, A. Kryczka, E. Malicka and B. Machura, *Dalton Trans.*, **54**, 2209 (2025); https://doi.org/10.1039/D4DT03237C
10. A.R. Al-Marhabi, R.M. El-Shishtawy, S.M. Bouzzine, M. Hamidi, H.A. Al-Ghamdi and K.O. Al-Footy, *J. Photochem. Photobiol. Chem.*, **436**, 114389 (2023); https://doi.org/10.1016/j.jphotochem.2022.114389
11. Bruker, APEX2 and SAINT. Bruker AXS Inc., Madison, Wisconsin, USA (2007).
12. Siemens Inc., SAINT, Area-Detector Integration Software, Version 6.01, Siemens. Industrial Automation, Inc., Madison, Wisconsin, USA (1997).
13. G.M. Sheldrick, SADABS: Siemens Area Detector Absorption Correction Program, Bruker Analytical X-ray Systems Inc., Madison, Wis, USA (2001).
14. R.H. Blessing, *Acta Crystallogr. A*, **51**, 33 (1995); https://doi.org/10.1107/S0108767394005726
15. T. Yanai, D.P. Tew and N.C. Handy, *Chem. Phys. Lett.*, **393**, 51 (2004); https://doi.org/10.1016/j.cplett.2004.06.011
16. M. Cossi, N. Rega, G. Scalmani and V. Barone, *J. Comput. Chem.*, **24**, 669 (2003); https://doi.org/10.1002/jcc.10189
17. G.M. Sheldrick, *Acta Crystallogr. A*, **64**, 112 (2008); https://doi.org/10.1107/S0108767307043930
18. G.M. Sheldrick, *Acta Crystallogr. C Struct. Chem.*, **71**, 3 (2015); https://doi.org/10.1107/S2053229614024218
19. A.L. Spek, *J. Appl. Cryst.*, **36**, 7 (2003); https://doi.org/10.1107/S0021889802022112
20. L.J. Farrugia, *J. Appl. Cryst.*, **30**, 565 (1997); https://doi.org/10.1107/S0021889897003117
21. R. Dennington, T. Keith and J. Millam, GaussView, Version 5, Semichem Inc., Shawnee Mission, KS, USA (2009).
22. A.D. Becke, *J. Chem. Phys.*, **98**, 5648 (1993); https://doi.org/10.1063/1.464913
23. P.R. Spackman, M.J. Turner, J.J. McKinnon, S.K. Wolff, D.J. Grimwood, D. Jayatilaka and M.A. Spackman, *Appl. Crystallogr.*, **54**, 1006 (2021); https://doi.org/10.1107/S1600576721002910
24. I. Fleming, Frontier Orbitals and Organic Chemical Reactions, Wiley-Blackwell: New York (1976).
25. S. Forli, R. Huey, M.E. Pique, M.F. Sanner, D.S. Goodsell and A.J. Olson, *Nat. Protoc.*, **11**, 905 (2016); https://doi.org/10.1038/nprot.2016.051
26. M.S. Hasson, A. Muscate, M.J. McLeish, L.S. Polovnikova, J.A. Gerlt, G.L. Kenyon, G.A. Petsko and D. Ringe, *Biochemistry*, **37**, 9918 (1998); https://doi.org/10.1021/bi973047e
27. D.T. Cremer and J.A. Pople, *J. Am. Chem. Soc.*, **97**, 1354 (1975); https://doi.org/10.1021/ja00839a011
28. M. Nardelli, *Acta Crystallogr. C*, **39**, 1141 (1983); https://doi.org/10.1107/S0108270183007696
29. A.R. Bassindale, *Tetrahedron*, **40**, 1019 (1984); https://doi.org/10.1016/S0040-4020(01)91219-3
30. M. Krishnaiah, N.J. Kumar, D.B. Reddy, M.M. Reddy, M. Soriano, Y.S. Chen and S.N. Rao, *Acta Crystallogr. C*, **51**, 2426 (1995); https://doi.org/10.1107/S010827019500583X
31. N. Ramasubbu and R. Parthasarathy, *Int. J. Pept. Protein Res.*, **34**, 153 (1989); https://doi.org/10.1111/j.1399-3011.1989.tb01505.x
32. J. Bernstein, R.E. Davis, L. Shimoni and N.L. Chang, *Angew. Chem. Int. Ed. Engl.*, **34**, 1555 (1995); https://doi.org/10.1002/anie.199515551
33. J.D. Roberts and M.C. Caserio, Basic Principles of Organic Chemistry W. A. Benjamin Inc., USA, edn 2 (1977).
34. V. Raj, D. Madheswari and M. Mubarak Ali, *J. Appl. Polym. Sci.*, **116**, 147 (2010); https://doi.org/10.1002/app.31511
35. T. Bruno and P. Svoronos, ^{13}C NMR Absorptions of Major Functional Groups, CRC Taylor Francis, Boca Raton, FL (2012).
36. S. Trabelsi, N. Kouki, M. Seydou, F. Maurel and B. Tangour, *ChemistryOpen*, **8**, 580 (2019); https://doi.org/10.1002/open.201800224
37. S. Gopalakrishnan, S. Vijayakumar and R. Shankar, *Struct. Chem.*, **29**, 1775 (2018); https://doi.org/10.1007/s11224-018-1156-7
38. H. Zhang, X. Wan, X. Xue, Y. Li, A. Yu and Y. Chen, *Eur. J. Org. Chem.*, **2010**, 1681 (2010); https://doi.org/10.1002/ejoc.200901167
39. K. Rajesh and P.P. Kumar, *Mater. Res. Express*, **4**, 016502 (2017); https://doi.org/10.1088/2053-1591/aa56cc
40. P. Naik, K.S. Keremane, M.R. Elmorsy, A. El-Shafei and A.V. Adhikari, *Electrochem. Sci. Adv.*, **2**, e2100061 (2022); https://doi.org/10.1002/elsa.202100061
41. K. Periyasamy, P. Sakthivel, G. Venkatesh, P. Vennila and Y. Sheena Mary, *Chem. Zvesti*, **78**, 447 (2024); https://doi.org/10.1007/s11696-023-03101-x
42. P.E. Kesavan, R.N. Behera, S. Mori and I. Gupta, *J. Fluoresc.*, **27**, 2131 (2017); https://doi.org/10.1007/s10895-017-2152-9
43. H.L. Hirshfeld, *Theor. Chim. Acta*, **44**, 129 (1977); https://doi.org/10.1007/BF00549096
44. U.M. Sumaya, E. Sankar, K.A. MohanaKrishnan, K. Biruntha and G. Usha, *Acta Crystallogr. E Crystallogr. Commun.*, **74**, 878 (2018); https://doi.org/10.1107/S2056989018007971
45. R. Eswaramoorthy, H. Hailekiros, F. Kedir and M. Endale, *Adv. Appl. Bioinform. Chem.*, **14**, 13 (2021); https://doi.org/10.2147/AABC.S290912
46. İ. Çapan, M. Hawash, N. Jaradat, Y. Sert, R. Servi and İ. Koca, *BMC Chem.*, **17**, 60 (2023); https://doi.org/10.1186/s13065-023-00961-y
47. S. Bhattacharya, C. Biswas, S.S.K. Raavi, J. Venkata Suman Krishna, N. Vamsi Krishna, L. Giribabu and V.R. Soma, *J. Phys. Chem. C*, **123**, 11118 (2019); https://doi.org/10.1021/acs.jpcc.9b01531